Redox Biology 13 (2017) 407–417

Contents lists available at ScienceDirect

Redox Biology

journal homepage: www.elsevier.com/locate/redox

Research Paper

Azidothymidine-triphosphate impairs mitochondrial dynamics by disrupting the quality control system

Ryosuke Nomura[a,b,1], Takeya Sato[a,*,1], Yuka Sato[a], Jeffrey A. Medin[c], Shigeki Kushimoto[b], Teruyuki Yanagisawa[a]

[a] Department of Molecular Pharmacology, Tohoku University Graduate School of Medicine, 2-1 Seiryo-machi, Aoba-ward, Sendai, Miyagi 980-8575, Japan
[b] Department of Emergency and Critical Care, Tohoku University Graduate School of Medicine, 1-1 Seiryo-machi, Aoba-ward, Sendai, Miyagi 980-8574, Japan
[c] Departments of Pediatrics and Biochemistry, Medical College of Wisconsin, 8701 Watertown Plank Road, CRI: C4540, Milwaukee, WI 53226, USA

ARTICLE INFO

Keywords:
Mitochondrial function
Mitochondrial dynamics
Oxidative stress
Metabolites
Oxidative phosphorylation
Cardiomyopathy

ABSTRACT

Highly active anti-retrovirus therapy (HAART) has been used to block the progression and symptoms of human immunodeficiency virus infection. Although it decreases morbidity and mortality, clinical use of HAART has also been linked to various adverse effects such as severe cardiomyopathy resulting from compromised mitochondrial functioning. However, the mechanistic basis for these effects remains unclear. Here, we demonstrate that a key component of HAART, 3'-azido-3'-deoxythymidine (AZT), particularly, its active metabolite AZT-triphosphate (AZT-TP), caused mitochondrial dysfunction, leading to induction of cell death in H9c2 cells derived from rat embryonic myoblasts, which serve as a model for cardiomyopathy. Specifically, treatment with 100 μM AZT for 48 h disrupted the mitochondrial tubular network via accumulation of AZT-TP. The mRNA expression of dynamin-related protein (*Drp)1* and the Drp1 receptor mitochondrial fission factor (*Mff*) was upregulated whereas that of optic atrophy 1 (*Opa1*) was downregulated following AZT treatment. Increased mitochondrial translocation of Drp1, Mff upregulation, and decreased functional Opa1 expression induced by AZT impaired the balance of mitochondrial fission vs. fusion. These data demonstrate that AZT-TP causes cell death by altering mitochondrial dynamics.

1. Introduction

Mitochondria are double-membrane organelles that play a critical role in cellular homeostasis. As such, mitochondrial quality control must be tightly regulated. Mitochondria are dynamic, mobile organelles that continuously change their shape and size through repeated cycles of fission (which allows the removal of damaged mitochondria) and fusion (to repair damaged components). In addition to morphological changes, mitochondrial dynamics include biogenesis, subcellular localization, and distribution [1,2]. These processes involve GTP hydrolysis and are important for maintaining normal cellular function. Fission is regulated by dynamin-related protein (Drp)1, a homolog of the GTP hydrolase (GTPase) dynamin that is involved in endocytosis, whereas fusion is mediated the GTPase dynamin-like proteins mitofusin (Mfn)1 and 2 and optic atrophy (Opa)1. These proteins regulate mitochondrial separation and thus control mitochondrial quality.

Antiretroviral drug combinations such as highly active anti-retrovirus therapy (HAART) have been developed to treat human immunodeficiency virus (HIV) infection. Long-term HAART is associated with adverse effects including myopathy, neuropathy, dyslipidemia, diabetes mellitus, pancreatitis, liver failure, and lipodystrophy [3–5]. The majority of HAART regimens involve nucleoside reverse transcriptase inhibitors (NRTIs) such as 3'-azido 3'-deoxythymidine (AZT) that can cause cardiomyopathy resulting from mitochondrial

Abbreviations: **ATP**, adenosine triphosphate; **AZT**, 3'-azido-3'-deoxythymidine; **AZT-DP**, AZT diphosphate; **AZT-MP**, AZT monophosphate; **AZT-TP**, AZT-triphosphate; **calcein-AM**, calcein acetoxymethyl ester; **cDNA**, complementary DNA; **DHE**, dihydroethidium; **DMEM**, Dulbecco's Modified Eagle Medium; **Drp1**, dynamin related protein-1; **FACS**, fluorescence-activated cell sorting; **FBS**, fetal bovine serum; **GAPDH**, glyceraldehyde 3-phosphate dehydrogenase; **GTP**, guanosine triphosphate; **GTPase**, guanosine triphosphate hydrolase; **HIV**, human immunodeficiency virus; **HPLC**, high-performance liquid chromatography; **HRP**, horseradish peroxidase; **HAART**, highly active antiretrovirus therapy; **IgG**, immunoglobulin G; **JC-1**, 5, 5′, 6, 6'-tetrachloro-1, 1', 3, 3'-tetraethybenzimidazolcarbocyanin iodide; **MA-5**, mitochonic asid-5; **Mff**, mitochondrial fission factor; **Mfn**, mitofusin; **mPTP**, mitochondrial permeability transition pore; **mtDNA**, mitochondrial DNA; **nDNA**, nuclear DNA; **NRTI**, nucleoside reverse transcriptase inhibitor; **OCR**, oxygen consumption rate; **Opa1**, optic atrophy 1; **PBS**, phosphate-buffered saline; **p-Drp1**, phosphorylated Drp1; **pol-γ**, DNA polymerase-gamma; **ROS**, reactive oxygen species; **TMPK**, thymidylate kinase; **WT**, wild type

* Corresponding author.
E-mail addresses: arumon-r@med.tohoku.ac.jp (R. Nomura), tksato@med.tohoku.ac.jp (T. Sato), yuka_dazzle_1201@yahoo.co.jp (Y. Sato), jmedin@mcw.edu (J.A. Medin), kussie@emergency-medicine.med.tohoku.ac.jp (S. Kushimoto), yanagswt@med.tohoku.ac.jp (T. Yanagisawa).
[1] These authors contributed equally to this work.

http://dx.doi.org/10.1016/j.redox.2017.06.011
Received 5 June 2017; Accepted 26 June 2017
Available online 29 June 2017

dysfunction, which can in turn worsen therapeutic outcomes [6,7]. Previous studies have shown that AZT causes changes to mitochondrial structure and respiratory chain enzyme activity, thereby reducing ATP levels [8,9].

AZT is a thymidine analog that is converted to an active triphosphate metabolite (AZT triphosphate, AZT-TP) by sequential phosphorylation [10]. Human thymidylate kinase (TMPK) catalyzes the conversion of AZT monophosphate (AZT-MP) to AZT diphosphate (AZT-DP), although the low conversion efficiency results in intracellular accumulation of AZT-MP [11], which is correlated with AZT toxicity [12]. In contrast, although the active metabolite AZT-TP exhibits antiretroviral activity, little is known about its toxicity to cells. We previously reported that TMPK mutants with improved AZT-MP conversion activity efficiently produced AZT-TP, the accumulation of which induced apoptosis [13], although the underlying mechanism remains to be elucidated.

To address this issue, the present study investigated the cardiotoxicity of AZT-TP using an H9c2 cell model established from rat embryonic myoblasts. We found that AZT-TP caused mitochondrial dysfunction, increased the production of cytotoxic reactive oxygen species (ROS), and impaired the balance of the mitochondrial quality control system.

2. Materials and methods

2.1. H9c2 cell culture

H9c2 rat embryonic myoblasts [14] were obtained from DS-Pharmaceutical (Osaka, Japan) and maintained in the Dulbecco's modified Eagle medium (DMEM; Wako Pure Chemical Industries, Osaka, Japan) supplemented with 10% fetal bovine serum (FBS; PAA Laboratories GmbH, Pasching, Austria), 100 U/ml of penicillin (Nacalai Tesque, Kyoto, Japan), and 100 μg/ml streptomycin (Nacalai Tesque) in an atmosphere of 37 °C and 5% CO_2 at constant humidity.

2.2. Preparation of recombinant lentivirus

We used a procedure for producing vesicular stomatitis virus-glycoprotein-pseudotyped recombinant lentivirus carrying human TMPK cDNA that was previously reported by our group [13,15]. Viral supernatant was harvested 48 h post-transfection and concentrated by ultracentrifugation at 72,500*g* for 2 h using an SW-28Ti swinging bucket rotor centrifuge (Beckman Coulter. Brea, CA, USA). Concentrated viral particles were resuspended in a small volume of DMEM containing 10% FBS. Viral titer was determined using 293 T cells. The percent expression of transgenes in 293T cells was determined 72 h post-infection by fluorescence-activated cell sorting (FACS) on a FACS Canto II instrument (BD Biosciences, Franklin Lakes, NJ, USA) after staining of the cells with phycoerythrin-labeled mouse monoclonal anti-human cluster of differentiation 19 antibody (BD Biosciences). Data were analyzed with Diva software (BD Biosciences).

2.3. Anti-TMPK antibody preparation

A rabbit polyclonal antibody against human TMPK was commercially generated (Sigma-Aldrich Japan, Tokyo, Japan) against the C-terminal 15 amino acids (199–212: CIRTATEKPLGELWK) of human TMPK conjugated with keyhole limpet hemocyanin.

2.4. Viral transduction and analysis of transgene expression by immunoblotting

H9c2 cells were transduced with viral stocks at a multiplicity of infection of 20 in the presence of 8 μg/ml protamine sulfate. Infected cells were cultured for 5 days, and transgene expression was confirmed by western blotting. Cells at 80% confluence were washed three times with chilled phosphate-buffered saline (PBS) composed of 10 mM phosphate buffer (pH 7.4) containing 150 mM NaCl and lysed with chilled radioimmunoprecipitation assay buffer containing a mixture of protease inhibitors (Nacalai Tesque) at 4 °C. The concentration of protein in the cell lysate was quantified with a bicinchoninic acid protein assay kit (Nacalai Tesque). Each sample (10 μg) was resolved by 12.5% sodium dodecyl sulfate-polyacrylamide gel electrophoresis and transferred to a polyvinylidene difluoride membrane that was probed with rabbit anti-human TMPK antibody (1: 5000) followed by horseradish peroxidase (HRP)-conjugated goat anti-rabbit immunoglobulin (Ig)G (1: 10,000; Cell Signaling Technology, Danvers, MA, USA). Loading of equal amounts of protein was confirmed using a murine anti-glyceraldehyde-3-phosphate dehydrogenase (GAPDH) antibody (1: 5000; Wako Pure Chemical Industries) followed by HRP-conjugated goat anti-mouse IgG (Cell Signaling Technology). Immunoreactivity was detected with the Immobilon Western Chemiluminescent HRP substrate (EMD Millipore, Billerica, MA, USA), and blots were imaged using a Chemidoc XRS system (Bio-Rad, Hercules, CA, USA) equipped with a charge-coupled device camera controlled by Image Lab software (Bio-Rad).

2.5. Analysis of intracellular metabolites of AZT

The procedure for analyzing intracellular concentrations of AZT metabolites has been previously described [13]. Briefly, cells were incubated with 500 μM AZT for 36 h, then resuspended in 5% (w/v) trichloroacetic acid, disrupted by sonication on ice, and centrifuged at 10,000 × *g* for 15 min at 4 °C to remove cell debris. The supernatant was neutralized by adding an equal volume of 20% tri-*n*-octylamine in pentane. The aqueous fraction was analyzed by high-performance liquid chromatography (HPLC).

2.6. Evaluation of AZT sensitivity in TMPK-expressing H9c2 cells

H9c2 cells expressing TMPK cDNA were seeded in 96-well plates (3×10^3/well) in 200 μl of cell culture medium containing increasing concentrations of AZT (0, 0.1, 1, 10, and 100 μM and 1 mM). After 4 days of culture, cell viability was analyzed using the Cell Titer-Glo cell viability assay kit (Promega, Madison, WI, USA).

To evaluate the effect of AZT on induction of apoptosis, cells seeded in 6-well plates (5×10^5/well) were cultured in the absence or presence of 100 μM AZT for 2 days, then stained with allophycocyanin-conjugated Annexin V (Bio Legend, San Diego, CA, USA) according to the manufacturer's protocol.

2.7. Fluorescence microscopy analysis of mitochondrial morphology in living cells

For live cell imaging of mitochondria, cells were stained with 100 nM MitoTracker Green (Invitrogen, Carlsbad, CA, USA) diluted with culture medium for 30 min at 37 °C, rinsed three times with PBS, and then transferred to a solution of Phenol Red-free DMEM (Wako Pure Chemicals Industries) supplemented with 10% FBS, antibiotics, and 25 mM HEPES-NaOH (pH 7.4). Mitochondrial morphology was analyzed by laser scanning confocal microscopy (LSM780; Zeiss, Oberkochen, Germany). The area of mitochondria was quantified using ImageJ software (National Institutes of Health, Bethesda, MD, USA) [16].

2.8. Determination of mitochondrial aspect ratio

Mitochondrial aspect ratio was determined as previously described [17,18]. Briefly, the MitoTracker Green signal in images was changed to a gray-scale image, and a suitable threshold level was set in ImageJ software to distinguish the signal intensities of mitochondria from background noise. The lengths of the major and minor axes of mitochondria were measured using ImageJ. The mitochondrial aspect

ratio was calculated as the ratio of the length of the major axis to that of the minor axis of mitochondria.

2.9. Evaluation of Drp1 translocation to mitochondria

Cells were seeded on glass cover slips and incubated with or without 100 μM AZT for 48 h. Mitochondria were then stained with 100 nM MitoRed (Dojindo Laboratories, Kumamoto, Japan) at 37 °C for 30 min and fixed with 4% formalin in PBS for 15 min at room temperature. To block non-specific binding of antibodies, the specimens were treated with blocking-permeabilization buffer containing 1% bovine

serum albumin fraction V (Sigma-Aldrich, St. Louis, MO, USA), 5% normal goat serum (Vector Laboratories, Burlingame, CA. USA), and 0.3% Triton X-100 (Sigma-Aldrich) in PBS for 1 h, followed by rabbit anti-Drp1 antibody (Cell Signaling Technology; 1:50 dilution in blocking permeabilization buffer) at 4 °C for 18 h. Samples were washed three times with PBS and then incubated with CF488A-conjugated goat anti-rabbit immunoglobulin G antibody (Biotium, Fremont, CA, USA; 1:500 dilution in PBS). Cell nuclei were stained with DAPI. Samples were mounted with Prolong Diamond Antifade Mountant (Molecular Probes, Eugene, OR, USA). Images of mitochondria were acquired to determine Drp1 localization using a structured illumination microscope with 100× CFI-SR Apochromat TIRF objective lens (NA = 1.49) (Nikon, Tokyo, Japan). Drp1 localization in mitochondria was evaluated by calculating the Pearson correlation coefficient using NIS Elements software (Nikon).

2.10. Quantitative real-time PCR

Total RNA was extracted from H9c2 cells using Sepazol reagent (Nacalai Tesque) according to the manufacturer's protocol. RNA concentration was quantified spectrophotometrically at a wavelength of 260 nm using a Nanodrop spectrophotometer (Nanodrop, Wilmington, DE, USA). cDNA synthesis and quantitative real-time PCR were performed using the ReverTra Ace and qPCR RT kits, respectively (Toyobo Co., Osaka, Japan). Briefly, RNA was reverse transcribed with ReverTra Ace reverse transcriptase according to the manufacturer's protocol, and PCR was performed using the Thunderbird SYBR qPCR master on an ABI Prism 7500 Sequence Detection System (Applied Biosystems, Foster City, CA, USA) according to the manufacturer's instructions. Relative expression levels of target genes were calculated with the $2^{-\Delta\Delta Ct}$ method relative to that of GAPDH, which was used as an internal control to correct for the total amount of RNA in each PCR reaction. Primer sequences are shown in Table 1 and were designed using the Primer3 program (National Center for Biotechnology Information, Bethesda, MD, USA).

2.11. Western blot analysis of Drp1, mitochondrial fission factor (Mff), and Opa1 expression in mitochondria

Mitochondria were isolated from cells treated with 100 μM AZT or left untreated for 48 h. The effect of AZT on Drp1 and Opa1 expression was analyzed by western blotting using antibodies against Drp1(1: 1000), Mff (1: 1000), and phosphorylated (p-)Drp1 (1: 1000) (all from Cell Signaling Technology) and against Opa1 (1: 2000; BD Biosciences). Equal protein loading was confirmed using a rabbit antibody against voltage-dependent anion channel (1:1000; Sigma-Aldrich).

Table 1
Primers used for quantitating expression levels of factors regulating mitochondrial dynamics and an internal control.

Target gene	Primer sequences
Rat Drp1	Forward: 5′-tgacatcttgaccgccatta-3′ Reverse: 5′-tgggctcctctagacgctta-3′
Rat Opa1	Forward: 5′-tcatggatccgaaagtgaca-3′ Reverse: 5′-atccttctgcagcaccaact-3′
Mff	Forward: 5′-acatgcgcattggagcagta-3′ Reverse: 5′-gccccactcaccaaatgaga-3′
Mfn2	Forward: 5′-tacgtgtatgagcggctgac-3′ Reverse: 5′-attatcccgggtgatgtcaa-3′
GAPDH	Forward: 5′-tgccactcagaaagactgtggatg-3′ Reverse: 5′-gcctgcttcaccaccttcttgat-3′

2.12. Measurement of mitochondrial oxygen consumption rate (OCR)

H9c2 cells expressing wild-type TMPK (hereafter referred to as WT TMPK) or the TMPK R16GLL mutant (hereafter referred to as mutant TMPK) were cultured in the absence or presence of 100 μM AZT for 24 h. Cells (5×10^4/well) were seeded in five wells of an XF24 cell culture plate (Seahorse Bioscience, North Billerica, MA, USA) and cultured for 24 h with or without 100 μM AZT. To measure mitochondrial OCR, we used the XF Cell Mito Stress Test kit (Seahorse Bioscience) according to the manufacturer's instructions. Briefly, the medium was changed to XF assay medium (Seahorse Bioscience) and after incubation for 1 h in a non-CO_2 incubator at 37 °C, OCR was measured using an XF24 Extracellular Flux Analyzer (Seahorse Bioscience). Cells were sequentially treated as follows: (a) basal respiration levels were monitored without additives; (b) oligomycin (1 μM) was added to reversibly inhibit ATP synthase and oxidative phosphorylation, revealing proton leakage; (c) the mitochondrial uncoupler carbonyl cyanide *p*-trifluoromethoxyphenylhydrazone (0.3 μM) was added to induce maximal respiration; and (d) the mitochondrial respiration inhibitors rotenone (0.1 μM; a complex I inhibitor) and antimycin A (0.1 μM; a complex III inhibitor) were added to terminate the reaction. OCR was calculated using Seahorse software (Seahorse Bioscience).

2.13. Measurement of mitochondrial inner membrane potential

Cells were treated with 100 μM AZT for 2 days or left untreated, and mitochondrial inner membrane potential was determined by staining with 200 nM of 5, 5′, 6, 6'-tetrachloro-1, 1', 3, 3'-tetraethylbenzimidazolylcarbocyanine iodide (JC-1; Molecular Probes) and measuring the fluorescence intensity by flow cytometry.

2.14. Evaluation of the effect of AZT on ROS production

Generation of mitochondrial ROS was measured by staining cells with dihydroethidium (DHE; Wako Pure Chemicals Industries). Superoxide anion radical converts DHE, a non-fluorescent dye, to the fluorescence-emitting 2-hydroxy ethidium [19]. Briefly, after 2 days of culture with or without 100 μM AZT, cells were incubated with 20 μM DHE for 30 min at 37 °C. The fluorescence intensity of DHE was analyzed by flow cytometry. The change in mean fluorescence intensity of cells in each treatment group is expressed as a percentage of the change in untreated control cells.

2.15. Mitochondrial permeability transition pore (mPTP) opening assay

The opening of the mPTP in H9c2 cells was measured with the calcein-cobalt mPTP assay [20]. Briefly, cells were washed with PBS and incubated with 2 μM calcein-acetoxymethyl ester (calcein-AM, Dojindo Laboratories, Kumamoto, Japan) at 37 °C for 20 min, then washed twice with PBS. The cells were then incubated with 5 mM $CoCl_2$ in PBS for 30 min at 37 °C to quench calcein-AM fluorescence and washed twice with PBS, and fluorescence intensity was measured by flow cytometry.

2.16. Quantification of nuclear (n)DNA and mitochondrial (mt)DNA copy numbers

Cells were treated with AZT for 2 days or left untreated and total DNA was isolated from cells using the SV Genomic DNA Isolation kit

Table 2
Primers used for quantification of mtDNA copy number.

Target gene	Primer sequences
Nicotinamide adenine dinucleotide hydride dehydrogenase (ND)1	Forward: 5′-acctcaccccttatcaacc-3′ Reverse: 5′-agggctccgaatagggagta-3′
Cytochrome oxidase (CO)1	Forward: 5′-ggagcagtattcgccatcat-3′ Reverse: 5′-cgacgaggtatccctgctaa-3′
Polymerase gamma 2 accessory subunit (PG2AS)	Forward: 5′-gatcaccaagaacagcagca-3′ Reverse: 5′-tacacaaggggtctccaag-3′

(Promega). Steady-state levels of mtDNA and nDNA were determined by real-time PCR. The copy number was normalized by calculating the mtDNA/nDNA ratio. Primer sequences are shown in Table 2 and were designed with the Primer3 program.

2.17. Statistical analysis

Data are presented as the mean ± SEM. Statistical analyses were performed using GraphPad Prism v.5 software (GraphPad Inc., La Jolla, CA, USA). One-way analysis of variance with the Bonferroni post-hoc test or Student's *t*-test was used to evaluate the statistical significance of mean differences, which was set at $P < 0.05$.

3. Results

3.1. Establishment of TMPK-overexpressing H9c2 cells

H9c2 cells were transduced with lentivirus at a multiplicity of infection of 20. We selected TMPK mutants that efficiently converted AZT-MP into AZT-DP with cells expressing WT TMPK serving as a control. Cell lysates were prepared 5 days after transduction and transgene expression was confirmed by western blotting (Fig. 1A, lanes 3 and 4; and Fig. 1B). In contrast, endogenous rat TMPK was detected at lower levels in the parental non-transduced H9c2 cell line (Fig. 1A, lane 1 and Fig. 1B) and transduction of H9c2 cells with mock lentivirus did not increase the expression of endogenous rat TMPK (Fig. 1A, lane 2 and Fig. 1B). Interestingly, higher molecular weight bands were observed for cells expressing mutant as compared to WT TMPK (Fig. 1A, lane 4). The mutant form of TMPK has high catalytic activity for

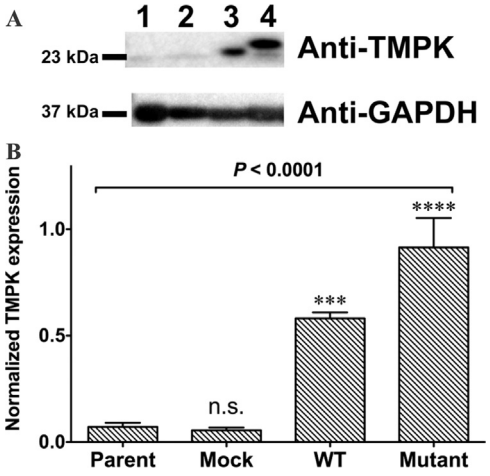

Fig. 1. TMPK expression in transduced H9c2 cells. A. TMPK expression in transduced H9c2 cells was examined by western blotting. GAPDH was used as a loading control. Lane 1, parental H9c2 cells; lane 2, cells transduced with LV/TMPK-WT; lane 3, cells transduced with LV/TMPK-mutant. **B.** Quantification of TMPK expression levels. Transduced cells showed higher TMPK expression than parental H9c2 cells. ***$P < 0.001$ and ****$P < 0.0001$ vs. parent. n.s., not significant vs. parent. Data represent mean ± SEM (n = 3). Statistical significance was evaluated by one-way analysis of variance with Bonferroni's multiple comparison post-hoc test.

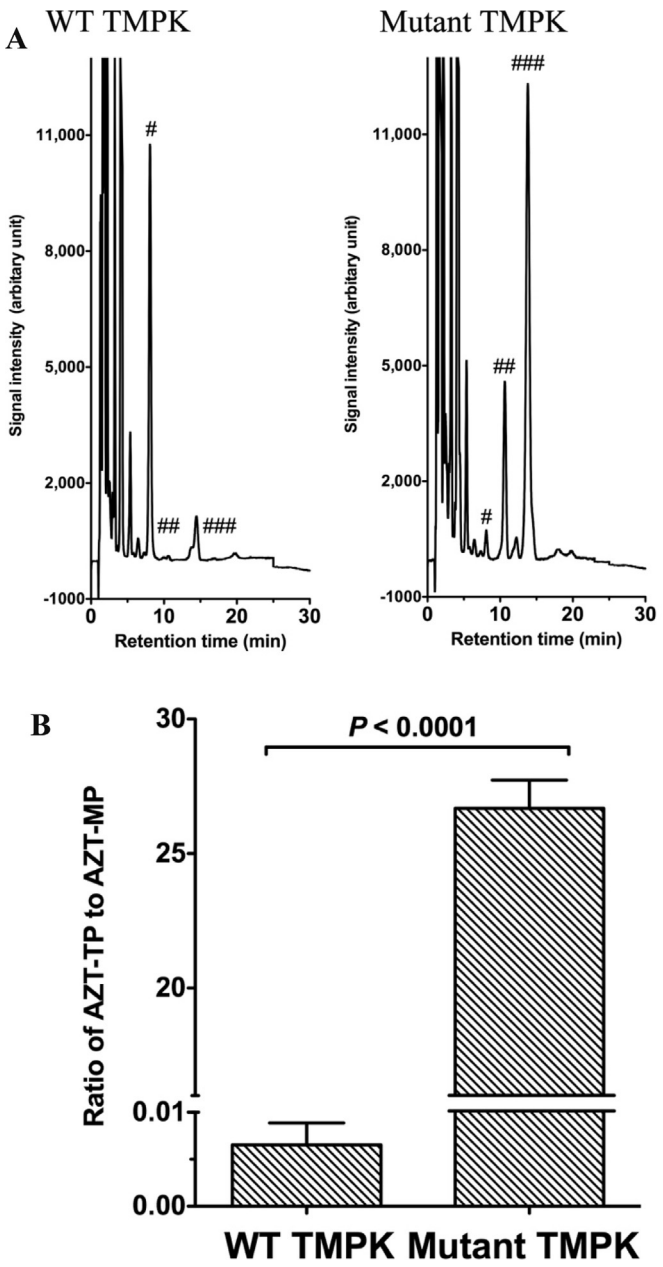

Fig. 2. AZT metabolite levels in TMPK-expressing H9c2 cells. A. Representative chromatograms of AZT metabolites extracted from H9c2 cells treated with 500 μM AZT for 36 h and analyzed using reverse-phase HPLC. Retention times of AZT-MP (#), AZT-DP (##), and AZT-TP (###) are shown. **B.** Comparison of the ratio of intracellular AZT metabolite levels in TMPK-expressing H9c2 cells. Data represent mean ± SEM (n = 6). Statistical significance was evaluated with Student's *t*-test.

conversion of AZT-MP to AZT-DP [11]; it transiently accepts the γ-phosphoryl group of ATP to generate an intermediate entity before the γ-phosphoryl group is transferred to AZT-MP to form AZT-DP. Hence, the higher molecular weight band of TMPK (Fig. 1A, lane 4) in the western blot may represent the intermediate form. WT TMPK-expressing cells showed a single band (Fig. 1A, lane 3).

3.2. Analysis of AZT metabolite accumulation

To confirm the functionality of TMPK expressed in transduced cells, we measured intracellular amounts of AZT metabolites by reverse-phase HPLC. Cells expressing mutant TMPK efficiently converted AZT-MP into AZT-DP and then into AZT-TP, a reaction that was catalyzed by endogenous nucleoside diphosphate kinase (Fig. 2A). To compare the

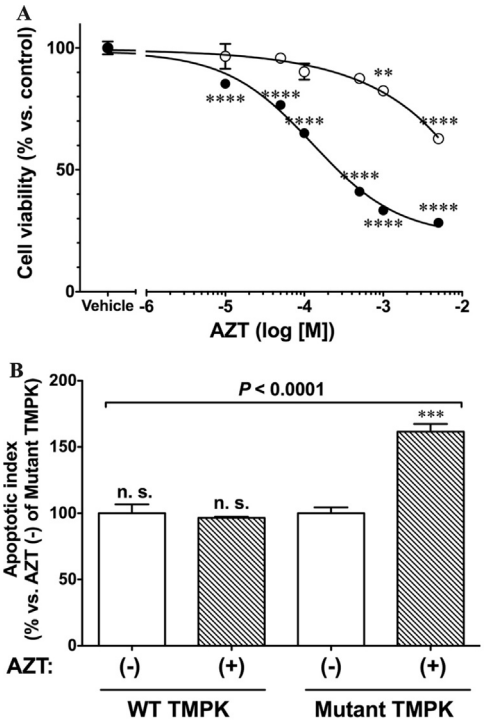

Fig. 3. Cell viability is decreased by active AZT metabolites. A. AZT-TP accumulation in mutant TMPK-expressing cells reduced cell viability in a concentration-dependent manner. Cells were cultured in the absence or presence of increasing concentrations of AZT for 48 h and viability was evaluated using the Cell Titer-Glo kit. Data represent mean ± SEM (n = 6). Statistical significance was evaluated by one-way analysis of variance with Bonferroni's multiple comparison post-hoc test. $^{**}P < 0.01$, $^{****}P < 0.0001$ vs. vehicle. ○: WT TMPK; •: Mutant TMPK. **B.** Mutant TMPK with 100 μM AZT treatment for 48 h increases apoptosis. Data represent mean ± SEM (n = 3). Statistical significance was evaluated by one-way analysis of variance with Bonferroni's multiple comparison post-hoc test. $^{***}P < 0.001$ vs. mutant TMPK without AZT.

amounts of AZT metabolites in cells, we calculated the ratio of AZT-TP to AZT-MP by measuring the areas under the curve of AZT-MP and AZT-TP from each chromatogram. Mutant TMPK-expressing cells showed a higher ratio of AZT-TP to AZT-MP than WT TMPK-expressing cells (Fig. 2B). These data demonstrate that AZT-TP accumulates in H9c2 cells expressing mutant TMPK.

3.3. Active AZT metabolites decrease cell viability

To investigate the effect of AZT antimetabolites on cell viability, TMPK-expressing cells were incubated with increasing concentrations of AZT for 4 days and cell viability was assayed based on cellular ATP levels (Fig. 3A). Cells expressing mutant TMPK showed a concentration-dependent decrease in viability in the presence of AZT, with a half-maximal inhibitory concentration of 70 μM. This was not observed in cells expressing WT TMPK and treated with up to 1 mM AZT. In subsequent experiments, cells were incubated with 100 μM AZT for 48 h.

We also evaluated the induction of apoptosis by AZT. Apoptosis was induced to a greater degree in cells expressing mutant but not WT TMPK treated with AZT (161.5 ± 5.88% vs. control, n = 3, P = 0.011) (Fig. 3B). These results indicate that AZT-TP is more toxic than AZT-MP to H9c2 cells.

3.4. AZT-TP accumulation causes mitochondrial fragmentation

Mitochondria are highly dynamic organelles that change their morphology depending on cellular demands to maintain their functionality, which is accomplished by the mitochondrial quality control system. We examined the effects of AZT on mitochondrial morphology by confocal microscopic live cell imaging. Mutant TMPK-expressing

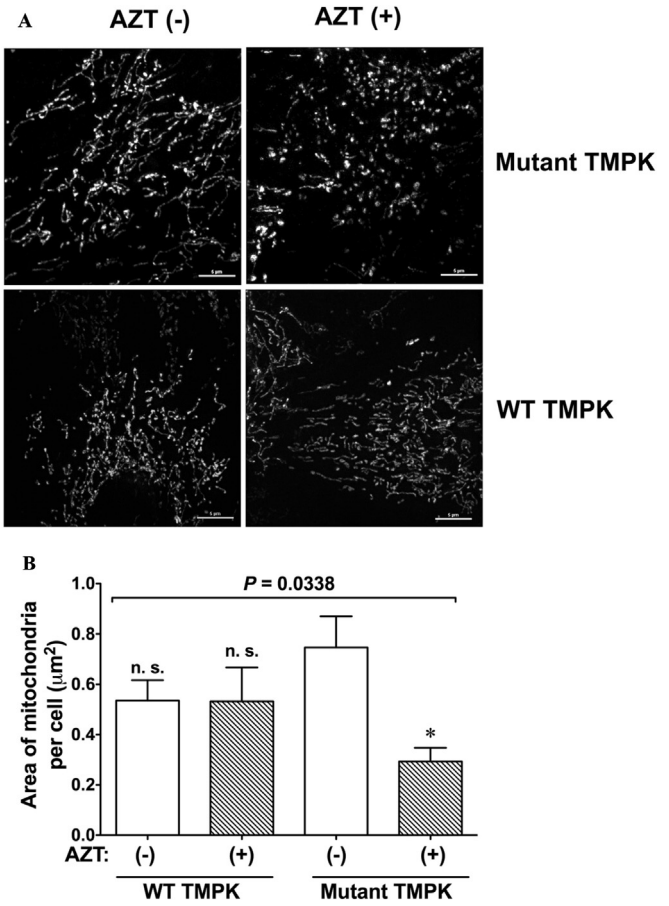

Fig. 4. Accumulation of AZT-TP but not AZT-MP disrupts the intracellular mitochondrial network. A. Mitochondrial network visualized by confocal microscopy after staining with 100 nM MitoTracker green. H9c2 cells expressing WT or mutant TMPK were treated with 100 μM AZT (+) or left untreated (−). Scale bar = 5 μm. **B.** Mitochondrial area per cell was decreased in mutant TMPK-expressing cells treated with AZT. $^{*}P < 0.05$ vs. mutant TMPK without AZT; n.s., not significant vs. mutant TMPK without AZT. Data represent mean ± SEM (n = 13). Statistical significance was evaluated by one-way analysis of variance with Bonferroni's multiple comparison post-hoc test. n.s.; not significant vs. mutant TMPK without AZT.

cells treated with AZT predominantly exhibited fission-like, fragmented mitochondria as compared to the network structure in untreated cells (Fig. 4A), suggesting that accumulation of the active AZT metabolite AZT-TP disrupts the mitochondrial network. We used ImageJ software to quantify the area of mitochondria in each image and found that it was smaller in mutant TMPK-expressing cells treated with AZT than in cells without treatment (Figs. 4B, 22.5 ± 2.05%, n = 8), whereas no difference was observed between WT TMPK-expressing cells in the presence and absence of AZT (Fig. 4B). We also measured the mitochondrial aspect ratio, which reflects the integrity of the mitochondrial network [17,18]. AZT treatment significantly decreased the ratio in mutant TMPK-expressing (80.6 ± 2.1% vs. untreated cells, P < 0.01, n = 20) but not in WT TMPK-expressing cells. These results indicate that AZT-TP accumulation causes mitochondrial fragmentation. For subsequent analyses of the expression of factors regulating mitochondrial dynamics, we examined mutant TMPK cells treated with AZT because WT TMPK cells did not show obvious changes.

3.5. Expression of the factors regulating mitochondrial dynamics is affected by AZT

Mitochondria form a complex network whose morphology is regulated through fission and fusion by four large GTPase family proteins, including Opa1, Mfn2, and Drp1, which is critical for maintaining

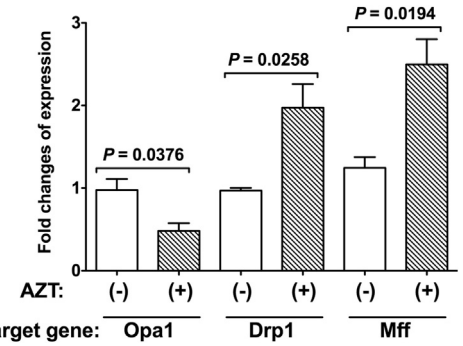

Fig. 5. Changes in expression levels of mitochondrial fission-fusion related factors induced by AZT. H9c2 cells expressing mutant TMPK were treated with 100 μM AZT (+) or left untreated (−) and changes in the expression of Opa1, Drp1, and Mff were measured by quantitative real-time PCR. Data represent mean ± SEM (n = 3). Statistical significance was evaluated with Student's *t*-test.

mitochondrial functions and cellular homeostasis. We examined the effects of AZT on the expression of these proteins by quantitative real-time PCR (Fig. 5) and western blotting (Fig. 6). AZT-TP accumulation caused downregulation of *Opa1* (Fig. 5, P = 0.0376, n = 3) and upregulation of *Drp1* (Fig. 5, P = 0.0258, n = 3); furthermore, *Mff* expression was increased by AZT treatment (Fig. 5, P = 0.0194, n = 3). In contrast, *Mfn2* expression was unaffected by AZT (data not shown).

To confirm these findings, we examined the expression levels of Opa1, Drp1, Mff and p-Drp1 by western blotting using isolated mitochondrial fractions prepared from mutant TMPK-expressing cells treated with AZT for 48 h or left untreated. Drp1 mainly exists in a phosphorylated form in the cytoplasm; its translocation to mitochondria is regulated by de-phosphorylation of p-Drp1 by calcineurin [21]. Opa1 was detected as two bands corresponding to the inner mitochondrial membrane-bound long form (Opa1-L, 90 kDa) and soluble short form (Opa1-S, 80 kDa). Opa1-S has been suggested as a mitochondrial fission factor [22]. AZT treatment decreased the ratio of Opa1-L to Opa1-S (Fig. 6A, $P = 0.0295$) and enhanced the expression of Drp1 (Fig. 6B, $P = 0.031$). The p-Drp-1/Drp-1 ratio in mitochondria was also reduced (Fig. 6D, $P = 0.0432$), suggesting that unphosphorylated Drp1 accumulated in mitochondria. Furthermore, the mitochondrial Drp1 receptor Mff was upregulated by AZT treatment (Fig. 6C, $P = 0.01$). We also explored Drp1 translocation to mitochondria following AZT treatment by immunohistochemistry using an anti-Drp1 antibody (Fig. 6E). After treatment with AZT, mitochondrial localization of Drp1 was increased in mutant TMPK-expressing cells (Fig. 6E). These results demonstrate that accumulation of AZT-TP disrupts the structure of the mitochondrial network by impairing the mitochondrial fission-fusion cycle.

3.6. AZT-TP accumulation impairs mitochondrial OCR

To confirm the effects of AZT on mitochondrial function in WT and mutant TMPK-expressing cells, we evaluated mitochondrial respiration by measuring OCR (Fig. 7A). AZT did not significantly alter basal OCR (Fig. 7B) or proton leakage (Fig. 7C) in cells expressing mutant and WT TMPK. However, the OCR in cells expressing mutant but not WT TMPK and treated with AZT was decreased, as evidenced by the reduced maximal respiratory capacity (Fig. 7D) relative to untreated controls ($P < 0.05$). These results indicate that the mitochondrial respiration system is damaged by AZT-TP but not by AZT-MP.

3.7. AZT causes collapse of mitochondrial membrane potential

AZT has been shown to cause mitochondrial dysfunction, resulting in myopathy [23]. To investigate the effect of AZT on mitochondrial function, we measured the change in mitochondrial membrane potential caused by AZT in TMPK-expressing cells using JC-1 (Fig. 8A). Unexpectedly, WT TMPK-expressing cells treated with AZT showed a decrease in mitochondrial membrane potential (Fig. 8A, $P = 0.0078$). This effect was even more pronounced in cells expressing the mutant kinase (Fig. 8A, $P < 0.0001$ vs. WT TMPK). These results indicate that the AZT metabolites AZT-MP and AZT-TP are both toxic to mitochondria, and that the latter has greater toxicity.

3.8. AZT-TP accumulation increases ROS production

ROS are mainly produced in mitochondria as a byproduct of respiration; excess ROS impairs cellular functions, leading to cell death. To assess the role of ROS in AZT-induced mitochondrial dysfunction, we measured mitochondrial ROS levels following treatment with 100 μM AZT for 2 days by staining cells with DHE, which reacts with ROS. We found that ROS production was increased by AZT in mutant TMPK-expressing cells ($P < 0.0001$) as compared to untreated controls (Fig. 8B). In contrast, AZT had no effect on WT TMPK-expressing cells.

3.9. AZT-TP accumulation increases mPTP opening

Cyclophilin D in the mitochondrial matrix is a member of the cyclophilin family of peptidyl prolyl-*cis, trans* isomerases that regulate protein folding [24,25], and has been reported to be involved in regulating mPT, which is a Ca^{2+}-dependent increase in the permeability of the mPTP to molecules < 1500 Da that results in decreased mitochondrial membrane potential, mitochondrial swelling, outer membrane rupture, and release of proapoptotic factors. Cyclosporin A is a specific inhibitor of cyclophilin family proteins that blocks mPTP opening. Given our observation that active AZT metabolites induced mitochondrial dysfunction, leading to induction of apoptosis, we examined whether metabolite accumulation increases the probability of mPTP opening. Cells expressing mutant TMPK treated with AZT showed an increase in mPTP opening (Fig. 8C, 132.1% ± 4.78%, n = 3) as compared to untreated cells ($P = 0.0026$), whereas those expressing WT TMPK showed a decrease in mPTP opening in the presence of AZT. These results suggest that accumulation of the active AZT metabolite AZT-TP induces mPTP opening, leading to loss of mitochondrial inner membrane potential.

3.10. AZT-TP accumulation does not affect mtDNA amount

Mitochondria have their own genomes encoding tRNA, rRNA, and protein sequences that maintain organelle functions. We speculated that the impairment of mitochondrial function by AZT treatment in mutant TMPK-expressing cells was due to a proportional reduction in mtDNA content. To test this hypothesis, we estimated mtDNA content by quantitative PCR. Cells were treated with AZT for 2 days or left untreated, and total DNA was isolated from cells; steady-state levels of mtDNA and nDNA were determined by real-time PCR and normalized by calculating the mtDNA/nDNA ratio. The normalized mean mtDNA copy number in both WT and mutant TMPK-expressing cells treated with AZT showed slight but non-significant decreases relative to untreated cells (Fig. 9), suggesting that AZT-TP does not affect the mtDNA content.

4. Discussion

HAART is a drug combination therapy that is used to disrupt the HIV life cycle and reduce morbidity and mortality caused by HIV infection. However, HAART can cause life-threatening clinical manifestations resulting from mitochondrial toxicity, such as myopathy and neuropathy [3–5]. NRTIs are a key component of HAART and are the main cause of mitochondrial toxicity occurring via inhibition of mitochondrial DNA polymerase (pol)-γ, which is essential for mtDNA synthesis [6,7,23]. However, the precise mechanism underlying the mitochondrial toxicity of NRTIs remains to be elucidated.

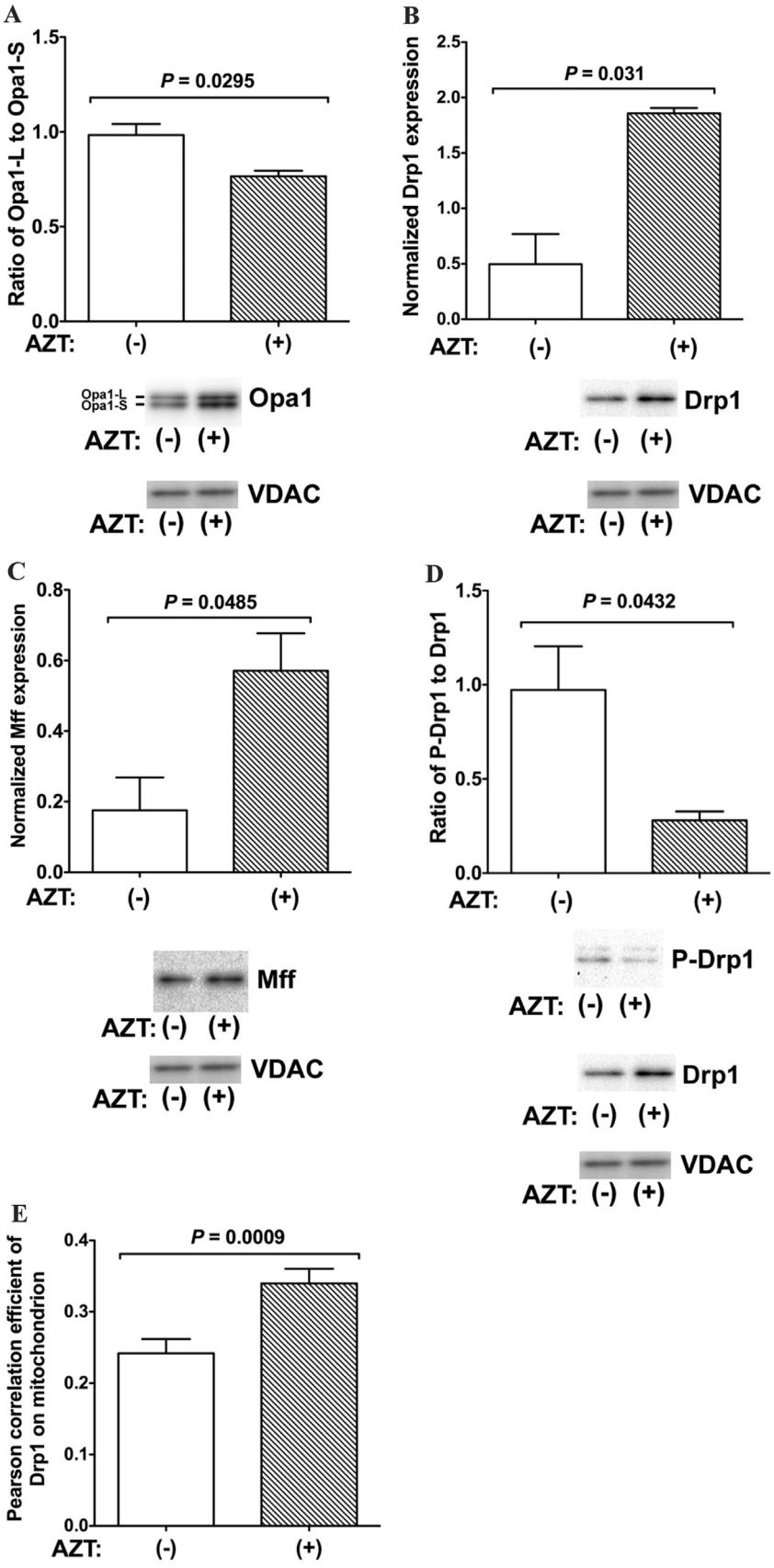

Fig. 6. Expression of factors related to mitochondrial fission and fusion in H9c2 cells expressing mutant TMPK. A–C. H9c2 cells expressing mutant TMPK were treated with 100 μM AZT (+) or left untreated (−) and changes in (A) the ratio of Opa1-L to Opa1-S and the expression of (B) Drp1 and (C) Mff relative to voltage-dependent anion channel (VDAC) were evaluated by western blotting. **D.** Mitochondrial translocation of Drp1 was increased by AZT treatment. The ratio of p-Drp1 to Drp1 is shown. Data represent mean ± SEM (n = 3). Statistical significance was evaluated with Student's *t*-test. **E.** Drp1 translocation to mitochondria was increased by treatment with 100 μM AZT, as determined by immunohistochemistry. Data represent mean ± SEM (n = 50). Statistical significance was evaluated with Student's *t*-test.

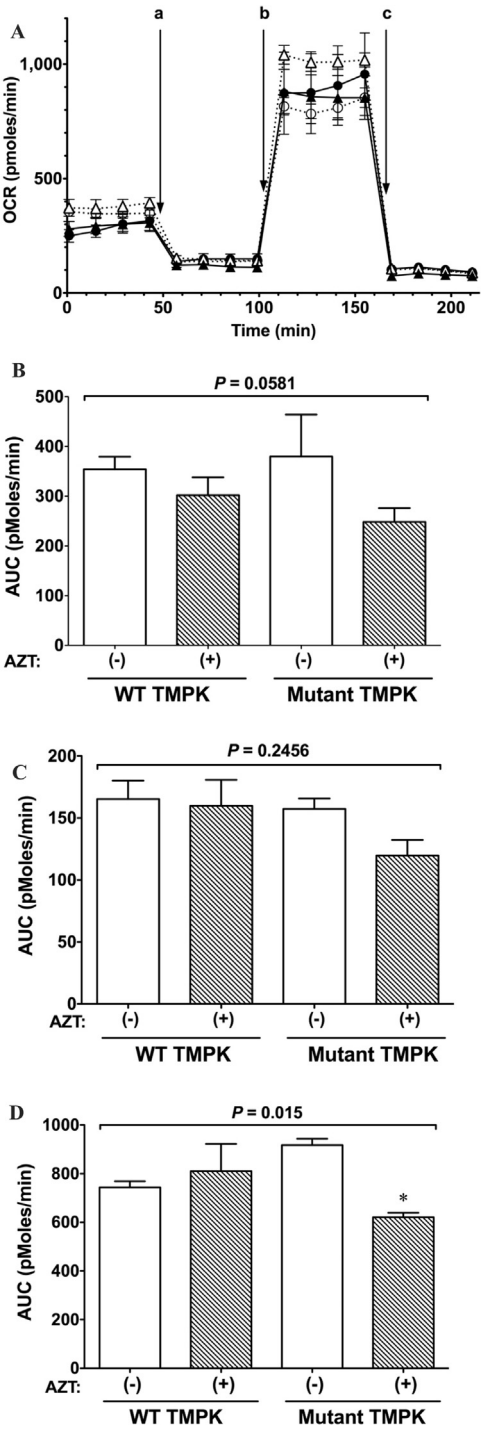

Fig. 7. Evaluation of mitochondrial respiration. A. Representative OCR profiles of H9c2 cells treated with 100 μM AZT or left untreated. After measurement of basal OCR, cells were sequentially incubated with 1 μM oligomycin to measure proton leakage (a); 0.3 μM carbonyl cyanide *p*-trifluoromethoxyphenylhydrazone to measure maximum respiration capacity (b); and 0.1 μM rotenone and 0.1 μM antimycin A to terminate the reaction (c). ○: WT TMPK without AZT; •: WT TMPK with AZT; △: mutant TMPK without AZT; ▲: mutant TMPK with AZT. Data represent mean ± SEM (n = 5). **B.** OCR (basal level). **C.** OCR following oligomycin addition. **D.** OCR of maximum respiratory capacity. Statistical significance was evaluated by one-way analysis of variance with Bonferroni's multiple comparison post-hoc test. $^{*}P < 0.05$ vs. mutant TMPK without AZT.

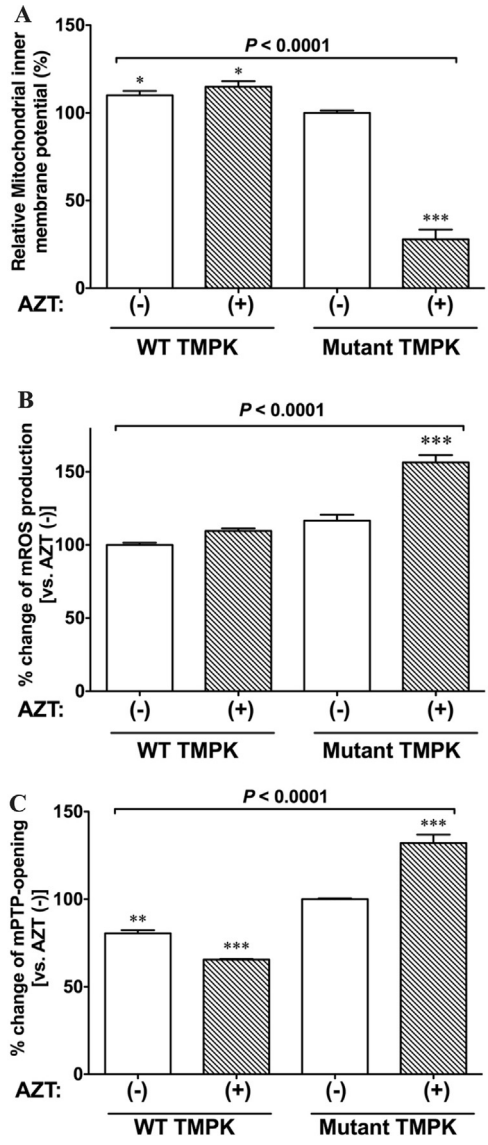

Fig. 8. AZT-TP accumulation causes mitochondrial dysfunction. A. AZT-TP accumulation severely decreases the mitochondrial membrane potential. H9c2 cells expressing WT or mutant TMPK were treated with 100 μM AZT (+) or left untreated (−) and mitochondrial membrane potential was monitored using the mitochondrial membrane potential sensor JC-1. The ratio of red to green JC-1 fluorescence intensity is shown. Data represent mean ± SEM (n = 3). $^{*}P < 0.05$ and $^{***}P < 0.0001$ vs. mutant TMPK without AZT (−). **B.** AZT-TP accumulation increases ROS production. H9c2 cells expressing WT or mutant TMPK were treated with 100 μM AZT (+) or left untreated (−) and ROS levels were measured with the superoxide anion-specific fluorescent probe DHE; fluorescence intensity data are shown as mean ± SEM (n = 3). $^{***}P < 0.0001$ vs. mutant TMPK without AZT (−). **C.** AZT-TP accumulation causes mPTP opening. H9c2 cells expressing WT or mutant TMPK were treated with 100 μM AZT (+) or left untreated (−) and mPTP opening was measured with the calcein-cobalt method and is shown as a relative percentage (means ± SEM) of the control (n = 3). $^{**}P < 0.001$ and $^{***}P < 0.0001$ vs. mutant TMPK without AZT (−). Statistical significance was evaluated by one-way analysis of variance with Bonferroni's multiple comparison post-hoc test.

Expression of mutant TMPK in H9c2 cells was previously shown to induce the phosphorylation of AZT-MP to overcome the rate-limiting step in AZT activation [11] and thereby increase AZT-DP and AZT-TP levels. This result is consistent with our previous report [13]. Although mitochondrial dysfunction caused by AZT has been attributed to the accumulation of the intermediate metabolite AZT-MP in cells, we found that AZT-TP was more toxic to H9c2 cells than AZT-MP [13], suggesting that AZT-TP is responsible for AZT toxicity. Based on our findings, we propose that H9c2 cells expressing TMPK are a useful model for examining the cardiotoxicity of AZT.

MtDNA replication occurs independently of the cell cycle [26], and its alteration can impair mitochondrial biogenesis and energy production, leading to organ dysfunction [27]. HAART has been linked to the dysregulation of mitochondrial biogenesis [28], whereas NRTIs have

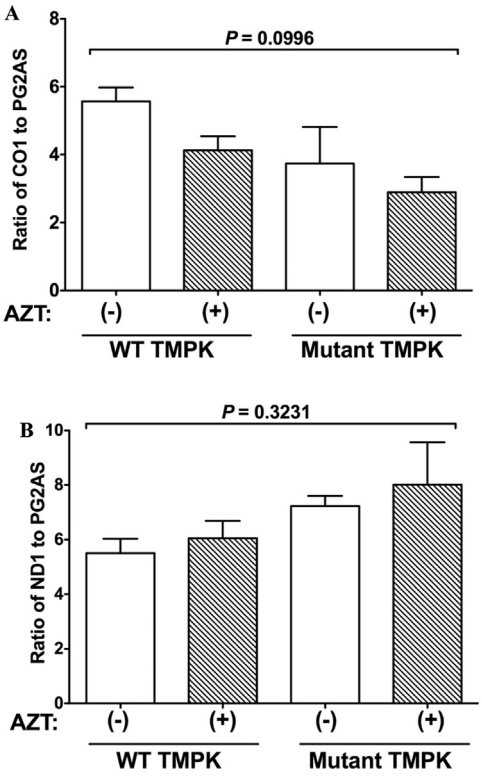

Fig. 9. Ratio of mtDNA/nDNA is unaffected by AZT treatment. H9c2 cells expressing WT or mutant TMPK were treated with 100 μM AZT (+) or left untreated (−). **A.** Ratio of cytochrome oxidase (CO)1 to polymerase gamma 2 accessory subunit (PG2AS). **B.** Ratio of adenine dinucleotide hydride dehydrogenase (ND)1 to PG2AS. Data represent mean ± SEM (n = 3). Statistical significance was evaluated by one-way analysis of variance with Bonferroni's multiple comparison post-hoc test.

been suggested to inhibit mitochondrial pol-γ [29]. NRTIs with a pyrimidine ring structure have been used in HIV/acquired immunodeficiency syndrome treatment to block the incorporation of endogenous nucleotides into nascent mtDNA; in fact, mtDNA depletion is a clinical symptom of NRTI toxicity [30]. In this study, we showed that treatment of mutant TMPK-expressing cells with 100 μM AZT did not deplete mtDNA (Fig. 9) despite evidence of mitochondrial dysfunction (Figs. 7 and 8), which was likely induced by AZT-TP accumulation prior to inhibition of mtDNA replication.

Transgenic mice expressing cardiac-specific genes are powerful tools for investigating the features of cardiac dysfunction, including HAART-associated cardiomyopathy and defects in mitochondrial quality control associated with drug toxicity [31]. One study reported a novel transgenic mouse line with cardiac-specific overexpression of human TMPK in which mtDNA was depleted and mitochondria showed ultrastructural damage, which was accompanied by increased left ventricular mass after 35 days of AZT treatment [32]. This is consistent with the previously described AZT-induced mitochondrial toxicity [33], but contradicts our results: we found that 2 days of AZT treatment did not significantly decrease mtDNA levels in H9c2 cells expressing mutant TMPK relative to control cells (Fig. 9). Although AZT-TP accumulation may cause mitochondrial dysfunction prior to depletion of mtDNA, further studies using both cells and transgenic mice are needed to clarify the underlying mechanisms. In addition, we observed that AZT-TP accumulation caused a decrease in mitochondrial respiratory function (Fig. 7) without decreasing mtDNA copy number (Fig. 9). We found that the increase in ROS production caused by AZT (Fig. 8B) decreased cell viability (Fig. 3) and the levels of complex 1 in mitochondria (T. Sato, unpublished data). It has been reported that AZT damaged mitochondrial complex 1 isolated from rat liver, leading to increased ROS production [34,35]. These observations suggest that AZT-TP may inhibit the assembly of proteins constituting the mitochondrial respiratory chain.

Furthermore, the observed decrease in oxidative stress in AZT-treated H9c2 cells induced by the antioxidant MitoTEMPO1 [36] and the fact that overexpression of mitochondrial superoxide dismutase in mice protects against AZT-induced cardiomyopathy [37] suggest that increased ROS production leads to mitochondrial dysfunction. In our study, the antioxidant *N*-acetylcysteine restored the viability of mutant TMPK-expressing cells that was reduced by AZT treatment (T. Sato, unpublished data).

AZT-TP accumulation caused mitochondrial fragmentation (Fig. 4A) in addition to dysfunction (Fig. 8A). Autophagy is a cellular process in which damaged organelles, including dysfunctional mitochondria in a process known as mitophagy, are engulfed by autophagosomes and delivered to the lysosome for degradation [38]. Stimulation of mitochondrial fission plays an important role in mitochondrial turnover. An imbalance between mitochondrial fission and fusion can affect mitochondrial morphology. Increasing fission while simultaneously suppressing fusion can induce mitophagy. Downregulation of Opa1 [39] or upregulation of Drp1 [40] has been shown to cause mitochondrial fragmentation, a precondition for mitophagy [41,42]; we observed this phenotype upon AZT treatment. The expression of *Opa1* was diminished by AZT treatment in H9c2 cells expressing mutant TMPK (Fig. 5); in contrast, the protein levels of both Opa1-L and S in mitochondria were slightly increased (Fig. 6A), although the difference in Opa1 expression with and without AZT treatment was not significant (data not shown). Additionally, the fission-related molecule Drp1 was upregulated and the ratio of Opa1-L to Opa1-S was decreased in mutant TMPK-expressing cells treated with AZT (Fig. 6A, B). We also observed similar changes in the ratio of Opa1-L to Opa1-S and in the expression of Drp1 in total cell lysates (Supplemental Fig. 1B, D). These results demonstrate that accumulation of AZT-TP, an active AZT metabolite, alters mitochondrial dynamics to promote mitophagy and alleviate cellular damage caused by excess ROS production from damaged mitochondria. The role of autophagy in AZT-induced mitochondrial dysfunction has been discussed in detail elsewhere (T. Sato et al., manuscript submitted).

Opa1 mediates mitochondrial fusion to preserve mitochondrial quality including cristae morphology, thereby protecting against cell death [43,44]. *Opa1* knockout mice die in utero [45], and *Opa1* deficiency causes mitochondrial fragmentation and dysfunction [46]. Mitochondrial Opa1-L is processed by zinc metalloprotease in conjunction with *m*-AAA protease to generate Opa1-S [47], which causes mitochondrial fragmentation when overexpressed [48]. Various types of stress can also induce the processing of Opa1-L to Opa1-S, leading to mitochondrial dysfunction [49].

Perturbation of the mitochondrial fission-fusion balance can aggravate ROS-induced tissue injury [50]. Accordingly, we found that increased accumulation of Opa1-S by AZT caused mitochondrial fragmentation (Fig. 6A). We also demonstrated that excessive ROS production was induced by AZT-TP accumulation in mutant TMPK-expressing cells (Fig. 8B). These results suggest that excess ROS enhances Opa1 processing and leads to mitochondrial fragmentation. Agents that scavenge excess ROS could be used to address whether ROS are required for Opa1 processing.

Given that NRTIs including AZT are a key component of current HAART regimens, minimizing NRTI-induced mitochondrial damage is critical. We recently reported that mitochonic acid (MA)-5 can rescue cell death caused by severe oxidative stress in human fibroblasts obtained from a patient with mitochondrial disease [51,52]. It is likely that MA-5 restores mitochondrial function impaired by the active AZT metabolite. We are now evaluating the effects of MA-5 on H9c2 cells expressing mutant TMPK and treated with AZT.

In summary, our data indicate that AZT-TP may interfere with the mitochondrial fission-fusion cycle by increasing ROS production, thereby disrupting the mitochondrial quality control system. The

adverse effects of AZT in patients treated with HAART over the long term should be reconsidered in light of the mitochondriopathy demonstrated in this study.

Funding sources

This work was supported by a Grant-in-aid for Scientific Research (C) by the Japan Society for the Promotion of Science (JSPS) KAKENHI (grant number 15K08226 to R.N.); JSPS KAKENHI (grant number 23618003 to T.S.); and by a Health and Labour Sciences Research Grant for research on/AIDS from the Ministry of Health Labour and Welfare (grant number 08004664 to T.S.).

Conflict of interest

The authors declare no conflict of interests.

Author contributions

R.N., T.S., S.K., and T.Y. designed the research; R.N., T.S., and Y.S performed the experiments; J.A.M. provided reagents and technical support; R.N., T.S., and T.Y. analyzed the data; and R.N. and T.S. wrote the paper.

Acknowledgments

The authors thank Drs. Qichao Song, Masaki Saito, and Noriko Toda for discussions and helpful suggestions regarding the data, and the Biomedical Research Core of Tohoku University Graduate School of Medicine and the Biomedical Research Unit of Tohoku University Hospital for their support.

Appendix A. Supplementary material

Supplementary data associated with this article can be found in the online version at http://dx.doi.org/10.1016/j.redox.2017.06.011.

References

[1] S.A. Detmer, D.C. Chan, Functions and dysfunctions of mitochondrial dynamics, Nat. Rev. Mol. Cell Biol. 8 (2007) 870–879.
[2] P. Amati-Bonneau, D. Milea, D. Bonneau, A. Chevrollier, M. Ferre, V. Guillet, N. Gueguen, D. Loiseau, M.A. de Crescenzo, C. Verny, V. Procaccio, G. Lenaers, P. Reynier, OPA1-associated disorders: phenotypes and pathophysiology, Int. J. Biochem. Cell Biol. 41 (2009) 1855–1865.
[3] M. Nagpal, V. Tayal, S. Kumar, U. Gupta, Adverse drug reactions to antiretroviral therapy in AIDS patients at a tertiary care hospital in India: a prospective observational study, Indian J. Med. Sci. 64 (2010) 245–252.
[4] W.T. Tadesse, A.B. Mekonnen, W.H. Tesfaye, Y.T. Tadesse, Self-reported adverse drug reactions and their influence on highly active antiretroviral therapy in HIV infected patients: a cross sectional study, BMC Pharmacol. Toxicol. 15 (2014) 32.
[5] A. Carr, J. Miller, M. Law, D.A. Cooper, A syndrome of lipoatrophy, lactic acidaemia and liver dysfunction associated with HIV nucleoside analogue therapy: contribution to protease inhibitor-related lipodystrophy syndrome, AIDS 14 (2000) F25–F32.
[6] A. Cossarizza, G. Moyle, Antiretroviral nucleoside and nucleotide analogues and mitochondria, AIDS 18 (2004) 137–151.
[7] C.A. Koczor, W. Lewis, Nucleoside reverse transcriptase inhibitor toxicity and mitochondrial DNA, Expert Opin. Drug Metab. Toxicol. 6 (2010) 1493–1504.
[8] M.T. Corcuera Pindado, A. Lopez Bravo, R. Martinez-Rodriguez, A. Picazo Talavera, F. Gomez Aguado, M. Roldan Contreras, M.J. Perez Alvarez, A. Fernandez Garcia, M.J. Alonso Martin, Histochemical and ultrastructural changes induced by zidovudine in mitochondria of rat cardiac muscle, Eur. J. Histochem. 38 (1994) 311–318.
[9] D.T. McCurdy 3rd, J.M. Kennedy, AZT decreases rat myocardial cytochrome oxidase activity and increases beta-myosin heavy chain content, J. Mol. Cell Cardiol. 30 (1998) 1979–1989.
[10] P.A. Furman, J.A. Fyfe, M.H. St Clair, K. Weinhold, J.L. Rideout, G.A. Freeman, S.N. Lehrman, D.P. Bolognesi, S. Broder, H. Mitsuya, Phosphorylation of 3′-azido-3′-deoxythymidine and selective interaction of the 5′-triphosphate with human immunodeficiency virus reverse transcriptase, Proc. Natl. Acad. Sci. USA 83 (1986) 8333–8337.
[11] A. Lavie, I.R. Vetter, M. Konrad, R.S. Goody, J. Reinstein, I. Schlichting, Structure of thymidylate kinase reveals the cause behind the limiting step in AZT activation, Nat. Struct. Biol. 4 (1997) 601–604.
[12] S.D. Sales, P.G. Hoggard, D. Sunderland, S. Khoo, C.A. Hart, D.J. Back, Zidovudine phosphorylation and mitochondrial toxicity in vitro, Toxicol. Appl. Pharm. 177 (2001) 54–58.
[13] T. Sato, A. Neschadim, M. Konrad, D.H. Fowler, A. Lavie, J.A. Medin, Engineered human tmpk/AZT as a novel enzyme/prodrug axis for suicide gene therapy, Mol. Ther. 15 (2007) 962–970.
[14] B.W. Kimes, B.L. Brandt, Properties of a clonal muscle cell line from rat heart, Exp. Cell Res. 98 (1976) 367–381.
[15] T. Sato, S. Ramsubir, K. Higuchi, T. Yanagisawa, J.A. Medin, Vascular endothelial growth factor broadens lentivector distribution in the heart after neonatal injection, J. Cardiol. 54 (2009) 245–254.
[16] R.K. Dagda, S.J. Cherra, S.M. Kulich, A. Tandon, D. Park, C.T. Chu, Loss of PINK1 function promotes mitophagy through effects on oxidative stress and mitochondrial fission, J. Biol. Chem. 284 (2009) 13843–13855.
[17] W.J. Koopman, H.J. Visch, S. Verkaart, L.W. van den Heuvel, J.A. Smeitink, P.H. Willems, Mitochondrial network complexity and pathological decrease in complex I activity are tightly correlated in isolated human complex I deficiency, Am. J. Physiol. Cell Physiol. 289 (2005) C881–C890.
[18] F. Valsecchi, S. Grefte, P. Roestenberg, J. Joosten-Wagenaars, J.A. Smeitink, P.H. Willems, W.J. Koopman, Primary fibroblasts of NDUFS4(-/-) mice display increased ROS levels and aberrant mitochondrial morphology, Mitochondrion 13 (2013) 436–443.
[19] L. Benov, L. Sztejnberg, I. Fridovich, Critical evaluation of the use of hydroethidine as a measure of superoxide anion radical, Free Radic. Biol. Med. 25 (1998) 826–831.
[20] V. Petronilli, G. Miotto, M. Canton, M. Brini, R. Colonna, P. Bernardi, F. Di Lisa, Transient and long-lasting openings of the mitochondrial permeability transition pore can be monitored directly in intact cells by changes in mitochondrial calcein fluorescence, Biophys. J. 76 (1999) 725–734.
[21] G.M. Cereghetti, A. Stangherlin, O. Martins de Brito, C.R. Chang, C. Blackstone, P. Bernardi, L. Scorrano, Dephosphorylation by calcineurin regulates translocation of Drp1 to mitochondria, Proc. Natl. Acad. Sci. USA 105 (2008) 15803–15808.
[22] R. Anand, T. Wai, M.J. Baker, N. Kladt, A.C. Schauss, E. Rugarli, T. Langer, The i-AAA protease YME1L and OMA1 cleave OPA1 to balance mitochondrial fusion and fission, J. Cell Biol. 204 (2014) 919–929.
[23] N. Apostolova, A. Blas-Garcia, J.V. Esplugues, Mitochondrial toxicity in HAART: an overview of in vitro evidence, Curr. Pharm. Des. 17 (2011) 2130–2144.
[24] D.R. Green, G. Kroemer, The pathophysiology of mitochondrial cell death, Science 305 (2004) 626–629.
[25] A.P. Halestrap, G.P. McStay, S.J. Clarke, The permeability transition pore complex: another view, Biochimie 84 (2002) 153–166.
[26] B. Pakendorf, M. Stoneking, Mitochondrial DNA and human evolution, Annu. Rev. Genom. Human. Genet. 6 (2005) 165–183.
[27] D.C. Wallace, Diseases of the mitochondrial DNA, Annu. Rev. Biochem. 61 (1992) 1175–1212.
[28] M.C. Dalakas, I. Illa, G.H. Pezeshkpour, J.P. Laukaitis, B. Cohen, J.L. Griffin, Mitochondrial myopathy caused by long-term zidovudine therapy, N. Engl. J. Med. 322 (1990) 1098–1105.
[29] W. Lewis, M.C. Dalakas, Mitochondrial toxicity of antiviral drugs, Nat. Med. 1 (1995) 417–422.
[30] G.P. Leung, Iatrogenic mitochondriopathies: a recent lesson from nucleoside/nucleotide reverse transcriptase inhibitors, Adv. Exp. Med. Biol. 942 (2012) 347–369.
[31] C. Koczor, J. Kohler, W. Lewis, Transgenic mouse models of mitochondrial toxicity associated with HIV/AIDS and antiretrovirals, Methods 51 (2010) 399–404.
[32] J.J. Kohler, S.H. Hosseini, I. Cucoranu, O. Zhelyabovska, E. Green, K. Ivey, A. Abuin, E. Fields, A. Hoying, R. Russ, R. Santoianni, C.M. Raper, Q. Yang, A. Lavie, W. Lewis, Transgenic cardiac-targeted overexpression of human thymidylate kinase, Lab. Investig. 90 (2010) 383–390.
[33] W. Lewis, I.L. Grupp, G. Grupp, B. Hoit, R. Morris, A.M. Samarel, L. Bruggeman, P. Klotman, Cardiac dysfunction occurs in the HIV-1 transgenic mouse treated with zidovudine, Lab. Investig. 80 (2000) 187–197.
[34] J. Pupure, M.A. Fernandes, M.S. Santos, A.J. Moreno, I. Kalvinsh, V. Klusa, C.R. Oliveira, Mitochondria as the target for mildronate's protective effects in azidothymidine (AZT)-induced toxicity of isolated rat liver mitochondria, Cell Biochem. Funct. 26 (2008) 620–631.
[35] Q. Sun, W. Zhong, W. Zhang, Z. Zhou, Defect of mitochondrial respiratory chain is a mechanism of ROS overproduction in a rat model of alcoholic liver disease: role of zinc deficiency, Am. J. Physiol. Gastrointest. Liver Physiol. 310 (2016) G205–G214.
[36] Y.M. Liu, E. Shim, P. Nguyen, A.T. Gibbons, J.B. Mitchell, M.C. Poirier, Tempol protects cardiomyocytes from nucleoside reverse transcriptase inhibitor-induced mitochondrial toxicity, Toxicol. Sci. 139 (2014) 133–141.
[37] J.J. Kohler, I. Cucoranu, E. Fields, E. Green, S. He, A. Hoying, R. Russ, A. Abuin, D. Johnson, S.H. Hosseini, C.M. Raper, W. Lewis, Transgenic mitochondrial superoxide dismutase and mitochondrially targeted catalase prevent antiretroviral-induced oxidative stress and cardiomyopathy, Lab. Investig. 89 (2009) 782–790.
[38] G. Twig, B. Hyde, O.S. Shirihai, Mitochondrial fusion, fission and autophagy as a quality control axis: the Bioenergetic view, Biochim. Biophys. Acta 1777 (2008) 1092–1097.
[39] O.J. Martin, L. Lai, M.M. Soundarapandian, T.C. Leone, A. Zorzano, M.P. Keller, A.D. Attie, D.M. Muoio, D.P. Kelly, A role for peroxisome proliferator-activated receptor gamma coactivator-1 in the control of mitochondrial dynamics during postnatal cardiac growth, Circ. Res. 114 (2014) 626–636.
[40] S. Wu, F. Zhou, Z. Zhang, D. Xing, Mitochondrial oxidative stress causes mitochondrial fragmentation via differential modulation of mitochondrial fission-fusion proteins, FEBS J. 278 (2011) 941–954.

[41] A. Tanaka, M.M. Cleland, S. Xu, D.P. Narendra, D.F. Suen, M. Karbowski, R.J. Youle, Proteasome and p97 mediate mitophagy and degradation of mitofusins induced by Parkin, J. Cell Biol. 191 (2010) 1367–1380.
[42] G. Twig, A. Elorza, A.J. Molina, H. Mohamed, J.D. Wikstrom, G. Walzer, L. Stiles, S.E. Haigh, S. Katz, G. Las, J. Alroy, M. Wu, B.F. Py, J. Yuan, J.T. Deeney, B.E. Corkey, O.S. Shirihai, Fission and selective fusion govern mitochondrial segregation and elimination by autophagy, EMBO J. 27 (2008) 433–446.
[43] C. Frezza, S. Cipolat, O. Martins de Brito, M. Micaroni, G.V. Beznoussenko, T. Rudka, D. Bartoli, R.S. Polishuck, N.N. Danial, B. De Strooper, L. Scorrano, OPA1 controls apoptotic cristae remodeling independently from mitochondrial fusion, Cell 126 (2006) 177–189.
[44] A. Olichon, E. Guillou, C. Delettre, T. Landes, L. Arnaune-Pelloquin, L.J. Emorine, V. Mils, M. Daloyau, C. Hamel, P. Amati-Bonneau, D. Bonneau, P. Reynier, G. Lenaers, P. Belenguer, Mitochondrial dynamics and disease, OPA1, Biochim. Biophys. Acta 1763 (2006) 500–509.
[45] V.J. Davies, A.J. Hollins, M.J. Piechota, W. Yip, J.R. Davies, K.E. White, P.P. Nicols, M.E. Boulton, M. Votruba, Opa1 deficiency in a mouse model of autosomal dominant optic atrophy impairs mitochondrial morphology, optic nerve structure and visual function, Hum. Mol. Genet. 16 (2007) 1307–1318.
[46] T. Varanita, M.E. Soriano, V. Romanello, T. Zaglia, R. Quintana-Cabrera, M. Semenzato, R. Menabò, V. Costa, G. Civiletto, P. Pesce, C. Viscomi, M. Zeviani, F. Di Lisa, M. Mongillo, M. Sandri, L. Scorrano, The OPA1-dependent mitochondrial cristae remodeling pathway controls atrophic, apoptotic, and ischemic tissue damage, Cell Metab. 21 (2015) 834–844.
[47] M. Kaser, M. Kambacheld, B. Kisters-Woike, T. Langer, Oma1, a novel membrane-bound metallopeptidase in mitochondria with activities overlapping with the m-AAA protease, J. Biol. Chem. 278 (2003) 46414–46423.
[48] N. Ishihara, Y. Fujita, T. Oka, K. Mihara, Regulation of mitochondrial morphology through proteolytic cleavage of OPA1, EMBO J. 25 (2006) 2966–2977.
[49] T. Wai, J. Garcia-Prieto, M.J. Baker, C. Merkwirth, P. Benit, P. Rustin, F.J. Rupérez, C. Barbas, B. Ibañez, T. Langer, Imbalanced OPA1 processing and mitochondrial fragmentation cause heart failure in mice, Science 350 (2015) aad0116.
[50] A.S. Gonzalez, M.E. Elguero, P. Finocchietto, S. Holod, L. Romorini, S.G. Miriuka, J.G. Peralta, J.J. Poderoso, M.C. Carreras, Abnormal mitochondrial fusion-fission balance contributes to the progression of experimental sepsis, Free Radic. Res. 48 (2014) 769–783.
[51] T. Suzuki, H. Yamaguchi, M. Kikusato, T. Matsuhashi, A. Matsuo, T. Sato, Y. Oba, S. Watanabe, D. Minaki, D. Saigusa, H. Shimbo, N. Mori, E. Mishima, H. Shima, Y. Akiyama, Y. Takeuchi, A. Yuri, K. Kikuchi, T. Toyohara, C. Suzuki, M. Kohzuki, J. Anzai, N. Mano, S. Kure, T. Yanagisawa, Y. Tomioka, M. Toyomizu, S. Ito, H. Osaka, K. Hayashi, T. Abe, Mitochonic acid 5 (MA-5), a derivative of the plant hormone indole-3-acetic acid, improves survival of fibroblasts from patients with mitochondrial diseases, Tohoku J. Exp. Med. 236 (2015) 225–232.
[52] T. Suzuki, H. Yamaguchi, M. Kikusato, O. Hashizume, S. Nagatoishi, A. Matsuo, T. Sato, T. Kudo, T. Matsuhashi, K. Murayama, Y. Ohba, S. Watanabe, S. Kanno, D. Minaki, D. Saigusa, H. Shinbo, N. Mori, A. Yuri, M. Yokoro, E. Mishima, H. Shima, Y. Akiyama, Y. Takeuchi, K. Kikuchi, T. Toyohara, C. Suzuki, T. Ichimura, J. Anzai, M. Kohzuki, N. Mano, S. Kure, T. Yanagisawa, Y. Tomioka, M. Toyomizu, K. Tsumoto, K. Nakada, J.V. Bonventre, S. Ito, H. Osaka, K. Hayashi, T. Abe, Mitochonic acid 5 binds mitochondria and ameliorates renal tubular and cardiac myocyte damage, J. Am. Soc. Nephrol. 27 (2016) 1925–1932.